The Astrophysical Journal, 824:6 (10pp), 2016 June 10 doi:10.3847/0004-637X/824/1/6

PTF13efv—AN OUTBURST 500 DAYS PRIOR TO THE SNHUNT 275 EXPLOSION AND ITS RADIATIVE EFFICIENCY

E. O. Ofek[1], S. B. Cenko[2], N. J. Shaviv[3,4], G. Duggan[5], N.-L. Strotjohann[1], A. Rubin[1], S. R. Kulkarni[5], A. Gal-Yam[1], M. Sullivan[6], Y. Cao[5], P. E. Nugent[7,8], M. M. Kasliwal[9], J. Sollerman[10], C. Fransson[10], A. V. Filippenko[8], D. A. Perley[11], O. Yaron[1], and R. Laher[12]

[1] Benoziyo Center for Astrophysics and the Helen Kimmel Center for Planetary Science, Weizmann Institute of Science, 76100 Rehovot, Israel
[2] Astrophysics Science Division, NASA Goddard Space Flight Center, Mail Code 661, Greenbelt, MD, 20771, USA
[3] Racah Institute of Physics, The Hebrew University, 91904 Jerusalem, Israel
[4] School of Natural Sciences, Institute for Advanced Study, Princeton NJ 08540, USA
[5] Cahill Center for Astronomy and Astrophysics, California Institute of Technology, Pasadena, CA 91125, USA
[6] School of Physics and Astronomy, University of Southampton, Southampton SO17 1BJ, UK
[7] Computational Cosmology Center, Lawrence Berkeley National Laboratory, 1 Cyclotron Road, Berkeley, CA 94720, USA
[8] Department of Astronomy, University of California, Berkeley, CA 94720-3411, USA
[9] Observatories of the Carnegie Institution for Science, 813 Santa Barbara Street, Pasadena CA 91101 USA
[10] Department of Astronomy, The Oskar Klein Centre, Stockholm University, AlbaNova University Centre, SE-106 91 Stockholm, Sweden
[11] Dark Cosmology Centre, Niels Bohr Institute, University of Copenhagen, Juliane Maries Vej 30, DK-2100 Copenhagen, Denmark
[12] Spitzer Science Center, MS 314-6, California Institute of Technology, Pasadena, CA 91125, USA
Received 2015 September 21; accepted 2016 March 7; published 2016 June 3

ABSTRACT

The progenitors of some supernovae (SNe) exhibit outbursts with super-Eddington luminosities prior to their final explosions. This behavior is common among SNe IIn, but the driving mechanisms of these precursors are not yet well-understood. SNHunt 275 was announced as a possible new SN during 2015 May. Here we report on pre-explosion observations of the location of this event by the Palomar Transient Factory (PTF) and report the detection of a precursor about 500 days prior to the 2015 May activity (PTF 13efv). The observed velocities in the 2015 transient and its 2013 precursor absorption spectra are low (1000–2000 km s^{-1}), so it is not clear yet if the recent activity indeed marks the final disruption of the progenitor. Regardless of the nature of this event, we use the PTF photometric and spectral observations, as well as *Swift*-UVOT observations, to constrain the efficiency of the radiated energy relative to the total kinetic energy of the precursor. We find that, using an order-of-magnitude estimate and under the assumption of spherical symmetry, the ratio of the radiated energy to the kinetic energy is in the range of 4×10^{-2} to 3.4×10^{3}.

Key words: stars: mass-loss – supernovae: general – supernovae: individual (PTF13efv, SNHunt275)

Supporting material: machine-readable tables

1. INTRODUCTION

Some supernova (SN) progenitors exhibit vigorous variability or possible explosive outbursts shortly (weeks to years) prior to the SN explosion (Foley et al. 2007; Pastorello et al. 2007; 2013, Fraser et al. 2013; Mauerhan et al. 2013; Ofek et al. 2013a, 2013b, 2014a; Margutti et al. 2014). SNe showing such activity are mostly of Type IIn (and Ibn), with spectra showing a blue continuum and hydrogen Balmer (and helium) emission lines (Schlegel 1990; Filippenko 1991, 1997; Pastorello et al. 2008; Kiewe et al. 2012). Moreover, it is possible that other classes of SNe also have precursors as well (e.g., Corsi et al. 2014; Strotjohann et al. 2015). Some of the SNe IIn are presumably powered by conversion of the large reservoir of kinetic energy to radiated energy via interaction of the ejecta with circumstellar material (CSM; e.g., Chugai & Danziger 1994; Svirski et al. 2012; Ofek et al. 2014b). We note that the classification of SNe IIn is not well-defined; some SNe display similar spectral features on timescales of a few days after the explosion, which subsequently disappear (Niemela et al. 1985; Fassia et al. 2001; Gal-Yam et al. 2014; Khazov et al. 2016; Shivvers et al. 2015; Smith et al. 2015; Yaron et al. 2016). It is possible that these flash-ionized SNe have lower CSM mass, and/or a CSM that is confined to short distances from the progenitor (e.g., Gal-Yam et al. 2014; Groh 2014; Yaron et al. 2016).

Ofek et al. (2014a) systematically searched for pre-explosion outbursts (precursors) among a sample of 16 SNe IIn in which the hydrogen Balmer lines persist at least until the SN maximum light. Five possible precursors were found. Based on this analysis, they conclude that precursor events among SNe IIn are common: assuming a homogeneous population, at the one-sided 99% confidence level, more than 98% of all SNe IIn have at least one pre-explosion outburst that is brighter than $3 \times 10^{7}\,L_{\odot}$ (absolute magnitude -14) that takes place up to 2.5 years prior to the SN explosion. The average rate of such precursor events during the year prior to the SN explosion is likely larger than one per year (i.e., multiple events per SN per year), and fainter precursors are possibly even more common. They also find possible correlations between the integrated luminosity of the precursor, and the SN total radiated energy, peak luminosity, and rise time. These correlations are expected if the precursors are mass ejection events, and the early-time light curve of these SNe is powered by interaction of the SN ejecta with optically thick CSM. No precursors were found in a similar search among five SNe IIn that was recently reported by Bilinski et al. (2015). They do not provide the absolute-magnitude-dependent search time of their sample, so direct comparison of the two surveys is not straightforward.

The nature of the SN precursors is unknown, although several theoretical mechanisms have been suggested to explain

this high mass-loss in the final stages of stellar evolution. These include the pulsational pair instability (e.g., Rakavy et al. 1967; Woosley et al. 2007; Waldman 2008; Moriya & Langer 2015), bursty shell oxygen burning (Arnett & Meakin 2011), binary evolution (e.g., Chevalier 2012; Soker & Kashi 2013), and internal gravity waves excited by core convection (Quataert & Shiode 2012; Shiode & Quataert 2014). In addition to the nature of the engine driving the precursors, another relevant question is how the mass-loss arises and the origin of the radiated luminosity. In the context of luminous blue variables and η Carinae in particular, one can envision mass-loss as arising from explosions—i.e., shock waves accelerating material at the surface, later converting the kinetic energy to radiation through the interaction of the freshly ejected material with previously ejected mass (e.g., Smith 2013). In this case, we expect the radiated energy to be less or comparable to the kinetic energy of the ejecta. In an opposite scenario, a super-Eddington radiative field drives mass through radiation pressure. Here we expect the radiated energy to be larger than the kinetic energy of the ejecta (Shaviv 2000, 2001).

SNHunt 275 (PSN J09093496+3307204) was discovered by Howerton.[13] Classification of the transient (Elias-Rosa et al. 2015) by the Asiago Transient Classification Program using a spectrum taken on 2015 February 9.93 (UTC dates are used throughout this paper) revealed a narrow P-Cygni Hα line with an emission width of about 900 km s^{-1} and an expansion velocity, derived from the absorption component, of 950 km s^{-1}. The P-Cygni profile is superposed on broad Hα emission, having a FWHM intensity of ~6800 km s^{-1}. Elias-Rosa et al. (2015) also reported on the detection of a possible source at the transient location in *Hubble Space Telescope* (*HST*) images with apparent magnitudes of 22.8, 21.5, and 22.5 (F606W filter) on 2009 February 9, 2008 March 30, and 2009 February 25, respectively. These correspond to absolute magnitudes of about −9.7, −11.0, and −10.0, respectively. Observations on 2015 March 9, April 9, and April 14 showed that the transient brightness had increased (de Ugarte Postigo et al. 2015a, 2015b, 2015c). Furthermore, spectroscopic observations on 2015 April 14 (with resolution $R \approx 500$) did not detect the P-Cygni absorption component. Vinko et al. (2015) reported that the absolute magnitude of the transient reached −17 on 2015 May 18, and suggested that the transient has exploded as a SN.

Here we present Palomar Transient Factory (PTF) observations of the field of this transient in the years prior to its recent discovery and the detection of a precursor event reaching an absolute magnitude of about −12 (Duggan et al. 2015). We use these observations to put limits on the ejected mass and the radiative efficiency of the precursor. The radiative efficiency is defined here as the ratio of the radiated energy to the kinetic energy. Although the results have an uncertainty of several orders of magnitude, they provide the foundations for better future measurements.

We assume a distance to the transient of about 30 Mpc and a Galactic reddening of $E_{B-V} = 0.023$ mag (Schlegel et al. 1998). In Section 2 we present our photometric and spectroscopic observations, as well as *Swift* observations. The results are discussed in Section 3 and summarized in Section 4.

[13] Submitted to the CBET confirmation page.

2. OBSERVATIONS

The Palomar Transient Factory (PTF and iPTF; Law et al. 2009; Rau et al. 2009), using the 48 inch Oschin Schmidt telescope, observed the field of SNHunt 275 starting in 2009 March. On 2013 December 12, PTF detected a new source at the location of the event, and the transient was named PTF 13efv (Figure 1). Spectroscopic classification obtained on 2013 December 13 suggested that this is a "SN imposter" (e.g., Van Dyk & Matheson 2012). All of the PTF observations are reduced using the PTF-IPAC pipeline (Laher et al. 2014) and the photometric calibration and magnitude system are described by Ofek et al. (2012a, 2012b).

Photometry of the source was derived using point-spread function fitting photometry on the subtracted images (see, e.g., Firth et al. 2015 for details). Three images obtained between 2014 January 23 and April 25 were used as a reference. The PTF *R*-band photometry is listed in Table 1 and the light curve is presented in Figure 2. The *R*-band light curve clearly shows a precursor detected toward the end of 2013 November. The first detection of this outburst was on 2013 November 26. The next observations, about two weeks later, do not show an indication for flux variations. Therefore, it is possible that the outburst started much earlier than November 26. Observations obtained on 2013 December 21 indicate that the source returned to the levels of the reference image. We note that our PTF *g*-band light curve includes a single nondetection on 2013 April 22 with a limiting magnitude of 21.1. The precursor disappeared in the third week of 2013 December. We note that in Figure 2 there is a single point, on 2009 September 10, that looks like an outburst. In order to test its reality, we ran the newly developed image subtraction code (Zackay et al. 2016) on the images, where we constructed a reference image using the optimal image coaddition algorithm described in Zackay & Ofek (2015a, 2015b). This image subtraction code is optimal in the background dominated noise limit, and unlike the popular image subtraction methods it is numerically stable, returns a subtraction image with uncorrelated noise, and preserves the shape of cosmic rays and bad pixels. We found out that the residual causing the detection on 2009 September 10 has a sharp shape, indicating that it is likely a bad pixel or radiation hit event. Therefore, we conclude that it is not an outburst.

We note that there are 21 observations obtained between 2010 February 13 and 16. All these observations have negative fluxes and their weighted mean count is -68 ± 9, where the error was estimated using the Bootstrap method (Efron 1982). This is likely due to real variability of the progenitor, specifically a decline in luminosity relative to the reference image. We note that the formal error on the mean (12 counts) is consistent with the bootstrap error. This consistency indicates that our error estimate is reasonable. For additional tests regarding systematics in our image subtraction and photometry we refer the reader to Ofek et al. (2014a).

Most of the optical spectra (see Table 2) were obtained with the Low Resolution Imaging Spectrometer (LRIS; Oke et al. 1995) on the Keck I 10 m telescope, although a few spectra were also taken with the DEep Imaging Multi-Object Spectrograph (DEIMOS; Faber et al. 2003) on the Keck II 10 m telescope, the Kast spectrograph (Miller & Stone 1993) on the Shane 3 m telescope at Lick Observatory, and the Gemini-North Multiobject Spectrograph (GMOS; Hook et al. 2004) on the 8 m Gemini-N telescope. Spectral reductions followed standard techniques (e.g., Matheson et al. 2000;

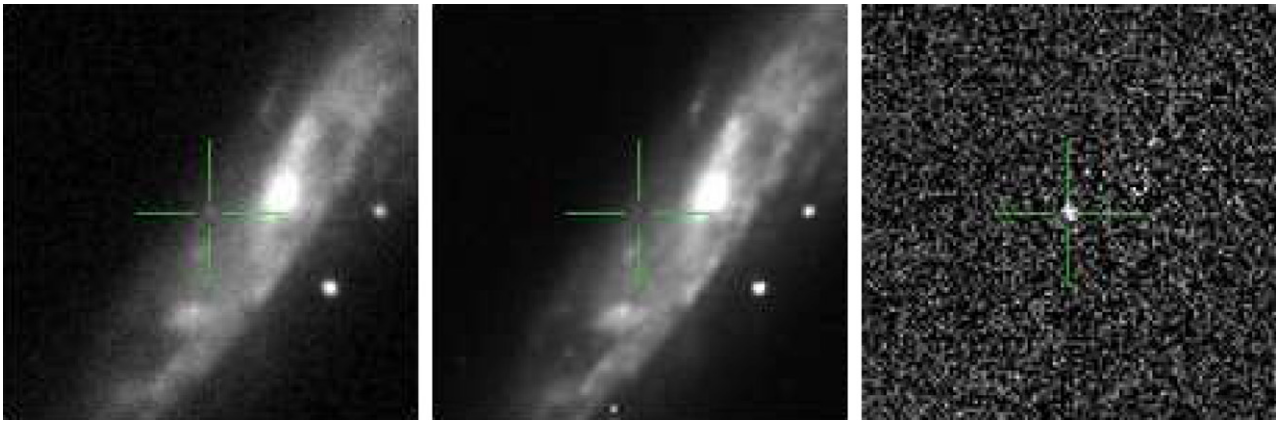

Figure 1. Image subtraction based detection of PTF 13efv from the PTF marshal. From left to right we show the new image, the reference image, and the subtracted image.

Silverman et al. 2012). All spectra are publicly available online via the Weizmann Interactive Supernova Data Repository, WISeREP[14] (Yaron & Gal-Yam 2012). The spectra are presented in Figure 3 and a close-up view of the Hα line is shown in Figure 4.

The first spectrum was obtained during the 2013 December outburst. It exhibits a strong and narrow Hα emission line (FWHM $\lesssim 500\,\mathrm{km\,s^{-1}}$) with a narrow P-Cygni absorption component at a velocity of $\sim$1300 km s^{-1} (measured relative to the peak of the emission line). The spectrum continuum is consistent with an effective temperature of about 5750 K and a radius of $\sim 4 \times 10^{14}$ cm (see Table 2). We note that, blueward of the Hα line, there is a minor decrement in the flux level. If this is due to a P-Cygni profile, in addition to the narrow P-Cygni at 1300 km s^{-1}, then this indicates velocities of up to 15,000 km s^{-1}. However, the nature of this decrement is not clear. The Hα luminosity at this epoch is roughly 1.2×10^{39} erg s^{-1}.

After the 2015 May rebrightening, the spectra become bluer, and the Hα emission line in the Keck/DEIMOS spectrum is well-described by a two-component Gaussian with component widths of $\lesssim$500 and $\sim$2000 km s^{-1}. A month later, the spectra become redder and two P-Cygni absorption features are detected in all of the Balmer lines: one with a velocity of $\sim$1000 km s^{-1} (as before), and a new absorption feature with a velocity of $\sim$2000 km s^{-1}. We note that the DEIMOS spectrum shows the Na I absorption doublet (5890, 5896 Å) at zero redshift and at the host-galaxy redshift. The equivalent width of the Na I doublet at the host-galaxy redshift is about 2.3 times stronger than the Galactic Na I absorption line. Therefore, it is likely that there is host-galaxy extinction in the direction of this event.

The Hα line luminosity as measured in the Keck/DEIMOS spectrum on 2015 May 20 is about 1.2×10^{40} erg s^{-1}. This is over an order of magnitude stronger than the luminosity during the 2013 outburst. We verified the flux calibration is correct by calculating the $V_{\rm UVOT}$-band synthetic magnitude from the spectrum and comparing it with the *Swift*-UVOT photometry.

SNHunt 275 exploded in NGC 2770, which has been the home of several SNe (e.g., Thöne et al. 2009), among which was SN 2008D (Soderberg et al. 2008; Modjaz et al. 2009). Thus, the host galaxy has been observed many times and by various instruments. Specifically, since 2008, it was observed by the Ultra-Violet/Optical Telescope (UVOT; Roming et al. 2005) on board the *Swift* satellite (Gehrels et al. 2004). Some of these observations have already been reported (e.g., Campana et al. 2015). The data were reduced using standard procedures (e.g., Brown et al. 2009). Flux from the transient was extracted from a 3″-radius aperture, with a correction applied to transform the photometry on the standard UVOT system (Poole et al. 2008). The resulting measurements, all of which have been converted to the AB system (Oke & Gunn 1983), are listed in Table 3 and displayed in Figure 5. Since there are no UVOT detections of the object prior to t_0 (=2457157.36, see definition below), Figure 5 shows only measurements taken after t_0. We note that the contribution from the host galaxy was subtracted by removing the (coincidence-loss corrected) mean count rate observed prior to 2015 January.

We used the UVOT observations to construct the bolometric light curve of the transient. This was done by correcting the measurements for Galactic reddening of $E_{B-V} = 0.023$ mag (Schlegel et al. 1998; Cardelli et al. 1989), and fitting a blackbody continuum to all of the observations in one-day bins (only in bins having observations in more than three bands). The fitted bolometric light curve, effective temperature, and radius are presented in Figure 6, while the fitted measurements are listed in Table 4. Figure 7 presents the UVOT spectral energy distribution, along with the best-fit blackbody curve, on three epochs, 1.8, 4.5, and 14.3 days after t_0. The uncertainties were estimated using the bootstrap method (Efron 1982) applied to each time bin. Following Ofek et al. (2014c), we further estimated the rise timescale of the event by fitting the luminosity (L) with an exponential rise of the form

$$L = L_{\rm max}(1 - \exp[-(t - t_0)/t_{\rm rise}]), \quad (1)$$

where $L_{\rm max}$ is the fitted maximum luminosity and t_0 is the fitted time of zero flux. We fitted the first four detections and estimate that $t_{\rm rise} \approx 2.2 \pm 1.6$ days, $L_{\rm max} = (2.0 \pm 0.3) \times 10^{42}$ erg s^{-1}, and $t_0 = 2,457,157.36 \pm 2.2$ day. We note that t_0 does not necessarily mark the time of explosion.

For each *Swift*-XRT image of the transient, we extracted the number of X-ray counts in the 0.2–10 keV band within an aperture of 9″ radius centered on the transient position. This aperture contains $\sim$50% of the source flux (Moretti et al. 2004). The background count rates were estimated in an annulus around the transient location, with an inner (outer) radius of 50″

[14] http://wiserep.weizmann.ac.il/

Table 1
PTF Photometric Observations

MJD (day)	Counts	Counts Error	Mag (mag)	Mag err. (mag)
54905.1661	−57.7	62.5	>21.32	⋯
54905.2811	36.5	56.0	>21.44	⋯
55084.5089	530.7	86.8	20.19	0.18
55087.5125	64.7	95.7	>20.85	⋯
55137.4415	−33.6	81.1	>21.03	⋯
55240.1202	−116.8	79.8	>21.05	⋯
55240.5060	−76.5	93.7	>20.88	⋯
55241.1410	−116.6	60.3	>21.36	⋯
55241.4996	−125.0	96.4	>20.85	⋯
55242.1389	−20.3	50.7	>21.54	⋯
55242.4967	−42.6	68.8	>21.21	⋯
55243.1236	−72.9	58.5	>21.39	⋯
55243.1739	−70.5	49.3	>21.58	⋯
55243.1756	−25.3	54.2	>21.47	⋯
55243.2207	−66.8	49.3	>21.58	⋯
55243.2223	−109.3	51.1	>21.54	⋯
55243.2676	−29.3	49.5	>21.57	⋯
55243.2694	−82.7	49.1	>21.58	⋯
55243.3150	−72.8	50.9	>21.54	⋯
55243.3167	−28.5	47.1	>21.62	⋯
55243.3610	−38.1	51.8	>21.52	⋯
55243.3628	−81.8	50.5	>21.55	⋯
55243.4087	−94.1	54.3	>21.47	⋯
55243.4105	−62.8	53.9	>21.48	⋯
55243.4544	−105.5	80.8	>21.04	⋯
55243.5096	−173.2	97.2	>20.84	⋯
56622.4310	439.6	109.9	20.39	0.27
56637.3456	303.0	115.6	>20.65	⋯
56637.3942	218.1	64.5	21.15	0.32
56638.4580	359.6	54.8	20.61	0.17
56638.4985	498.0	63.1	20.26	0.14
56638.5411	412.3	56.6	20.46	0.15
56639.2757	241.3	111.5	>20.69	⋯
56639.3197	278.1	84.9	20.89	0.33
56639.3600	277.3	69.6	20.89	0.27
56639.4031	252.7	71.8	20.99	0.31
56639.4473	336.7	63.0	20.68	0.20
56639.4895	287.7	52.9	20.85	0.20
56639.5333	283.7	54.3	20.87	0.21
56640.4351	391.6	133.3	>20.50	⋯
56640.4606	315.5	163.7	>20.27	⋯
56640.4854	293.8	130.7	>20.52	⋯
56647.4823	61.8	120.0	>20.61	⋯
56647.5074	−159.5	114.1	>20.66	⋯
56647.5221	−46.0	117.0	>20.64	⋯

Note. Image-subtraction-based *R*-band photometry of PTF 13efv. MJD is the modified Julian day. AB Magnitudes are presented as lower limits when the detection is less than 3σ than the noise level. The count rate can be converted to AB magnitude with $M = 27 - 2.5 \log_{10}(\text{Counts})$.

(This table is available in machine-readable form.)

(100″). The log of *Swift*-XRT observations, along with the source and background X-ray counts in the individual observations, is given in Table 5. While binning the observations in 10-day bins, we did not detect X-rays from this position with a false-alarm probability lower than 4%. In the two weeks after t_0, we can set a 2σ upper limit of 0.26 count ks^{-1} in the 0.2–10 keV range. Assuming a Galactic neutral hydrogen column density of $n_{\rm H} = 1.8 \times 10^{20}$ cm^{-2} and an intrinsic power-law spectrum with a photon index of $\Gamma = 2$,

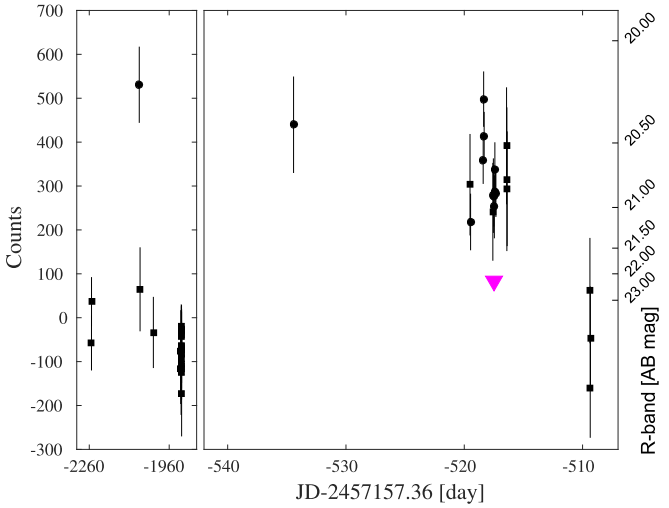

Figure 2. PTF light curve at the position of SNHunt 275 prior to its 2015 May event. Black filled symbols represent the PTF measurements. Circles mark individual measurements that are three times above the noise level, while squares represent measurements that are consistent with three times the noise. The triangle marks a *Swift*-UVOT *UM2* upper limit. We note that the weighted mean of the counts during the 2013 outburst is 326 ± 18.

this translates to an upper limit on the luminosity of $L_X < 1.1 \times 10^{39}$ erg s^{-1} within the *Swift*-XRT energy range.

Throughout this paper we assume a distance to SNHunt 275 of 30 Mpc (distance modulus 32.38 mag). The reduction and analysis presented here is based mainly on tools available as part of the MATLAB astronomy and astrophysics package (Ofek 2014).

3. DISCUSSION

Here, we briefly review the properties of the 2013 event (Section 3.1), and discuss the question of whether SNHunt 275 marks the final disruption of the star (Section 3.2). Furthermore, by analyzing the properties of the 2013 precursor and the latest explosion (2015 May), we attempt to constrain the physical setup of this explosion, and specifically the radiative efficiency of the precursor explosions (Section 3.3). In Section 3.4 we discuss the question of whether the possible mass-loss is driven by a radiation field, or the radiation is generated by the mass-loss interaction with previously emitted material.

3.1. The 2013 Event

To summarize, the 2013 outburst took place about 500 days prior to the 2015 May main event and reached a peak absolute magnitude of about −11.9 in the *R*-band ($\approx 1.7 \times 10^{40}$ erg s^{-1}). The duration of this outburst was longer than 20 days, hence the integrated radiated energy in the *R*-band is $>2.4 \times 10^{46}$ erg. An interesting fact is that the outbursts decayed fast, on a timescale of a week. A spectrum taken during the outburst revealed Balmer lines with a P-Cygni profile with a velocity of about 1000 km s^{-1}. These properties are summarized in Table 6.

In terms of peak absolute magnitude and the total radiated energy, this event is at the low end of the precursor event population reported in Ofek et al. (2014a). However, this is a clear selection bias. One of the most well-studied SNs showing multiple precursor events is SN 2009ip (Smith et al. 2010; Mauerhan et al. 2013; Ofek et al. 2013a; Pastorello et al. 2013;

Table 2
Log of Spectroscopic Observations

Telescope	Instrument	Setup	MJD	Temp. (K)	Radius (cm)
Gemini-N	GMOS	R400/G5305	56639.8	5820	4×10^{14}
Keck I	LRIS	400/3400, 400/8500	57158.3	10,800	6×10^{14}
Keck I	LRIS	400/3400, 400/850	57162.3	9230	4×10^{14}
Keck II	DEIMOS	1200G	57162	9030	7×10^{14}
Keck I	LRIS	400/3400, 400/8500	57186.3	6010	1×10^{15}
Keck I	LRIS	600/4000, 1200/7500	57189	...	...
Lick 3 m	Kast	600/4310, 300/7500	57191	5960	1×10^{15}

Note. MJD is the modified Julian day. The temperature and radius are based on fitting a blackbody continuum to the spectra (excluding the Hβ and Hα regions). Since the temperatures may be affected by metal absorption, they should be regarded as lower limits. Similarly, the radii should be regarded as upper limits. "Setup" indicates the grating name, or (respectively) the blue grism and red grating. The spectra were obtained at the parallactic angle, and were corrected for airmass-effects using the mean atmospheric extinction curve for each site. We note that the Galactic reddening ($E_{B-V} = 0.023$ mag) is taken into account in the effective temperature calculations. However, we ignored the unknown host extinction. If the host extinction is indeed a factor of two larger than the Galactic extinction, as suggested by the Na I absorption doublet, then the lower limit on the effective temperature will be 300–1000 K higher than that listed in the table.

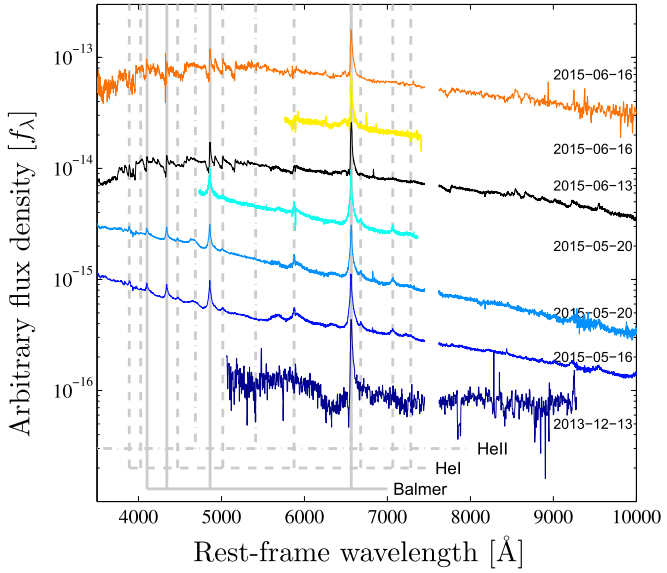

Figure 3. Spectra of PTF 13efv/SNHunt 275 obtained as part of the PTF project. The spectra are corrected for the host-galaxy redshift. The 2013 December 13 spectrum is smoothed using a five-pixel median filter. Telluric line regions were removed from the spectra.

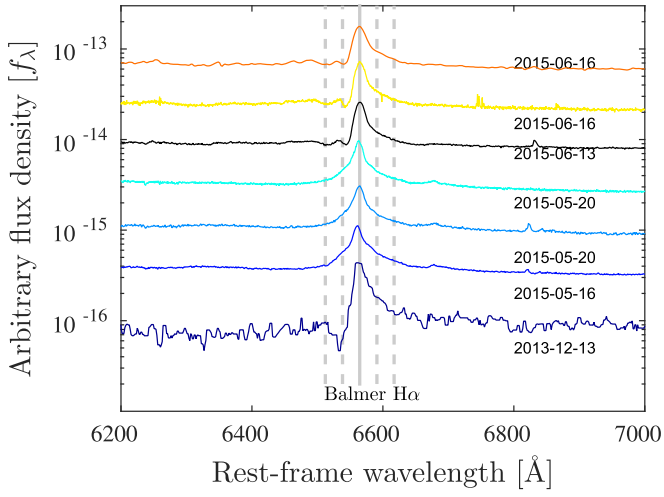

Figure 4. Close-up view of the Hα region of the PTF spectra (Figure 3). The solid vertical line represents the rest-frame wavelength of the Hα line, while the dashed lines are for velocities of 1000 and 2000 km s^{-1}. On 2015 June a double absorption P-Cygni profile, with velocities of 1000 and 2000 km s^{-1}, appears.

Prieto et al. 2013; Fraser et al. 2015). Interestingly, SN 2009ip likely showed four events, prior to its presumably final explosion on 2012 September (e.g., Smith et al. 2010). These events took place at about −25, −660, −710, and −1060 days prior to the latest explosion. The activity of SNHunt 275 on timescales of tens to hundreds of days prior to the presumably final explosion is similar to the one observed in SN 2009ip. One difference is that the peak luminosity of the outbursts seen in SN 2009ip was about an order of magnitude higher than that of SNHunt 275. One key question that is not yet clear in the cases of SN 2009ip and SNHunt 275 is if we saw the final death of the star, or the latest events are just other outbursts that are brighter than average.

3.2. The Nature of the 2015 Event

A close-up view of the evolution of the Hα line is presented in Figure 4. An interesting fact is the appearance of a single

Table 3
Swift-UVOT Photometric Observations

Filter	JD − t_0 (day)	Counts	Counts error
V	−2685.8316	−0.016	0.054
V	−2682.2874	0.087	0.074
V	−2680.7415	−0.007	0.040
V	−2679.6697	0.004	0.052
V	−2678.8016	0.000	0.047

Note. Time is given relative to $t_0 = 2{,}457{,}157.36$. The counts are background-subtracted, where the background is estimated as the mean of all the observations in a given filter obtained before 2015 January 1. The subtracted backgrounds are 0.892, 1.496, 0.743, 0.085, 0.206, and 0.146 counts for the *V*, *B*, *U*, *UVM*2, *UVW*1, and *UVW*2 filters, respectively. The zero points to convert these counts to AB magnitudes are 17.88, 18.99, 19.36, 18.97, 18.53, and 19.07 mag, for the *V*, *B*, *U*, *UVW*1, *UVM*2, and *UVW*2 filters, respectively.

(This table is available in its entirety in machine-readable form.)

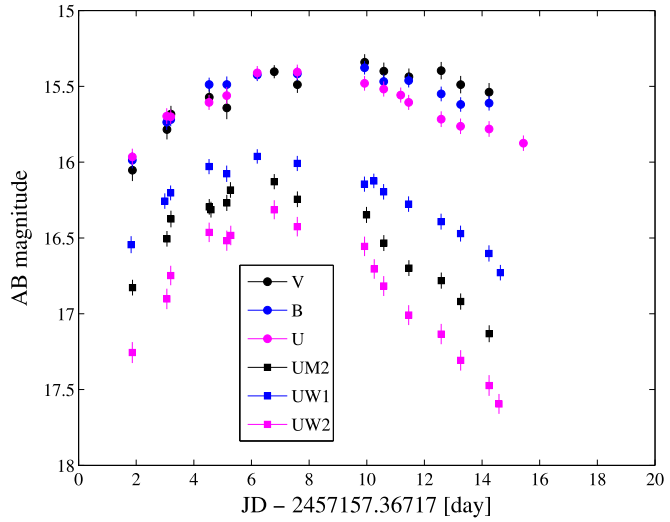

Figure 5. *Swift*-UVOT apparent magnitude light curves (not corrected for extinction) in the *UW2*, *UW1*, *UM2*, *U*, *B*, and *V* bands. The host contributions, estimated based on images taken prior to 2015 January, are subtracted (see the Table 3 caption). Precursors are not detected in observations prior to the 2015 May event. The full list of photometric measurements from 2008 until 2015 appears in Table 3.

P-Cygni absorption feature during the 2013 outburst, and two absorption features in spectra taken about one month after the 2015 May event. This double P-Cygni absorption feature, with ~1000 and ~2000 km s^{-1} velocities, is seen in all of the Balmer lines in the spectrum.

This can be interpreted in several ways; here we mention two obvious possibilities. First, the absorption at 2000 km s^{-1} can be produced by material ejected after the 2013 outburst but before the 2015 May event (e.g., during the 2015 February rebrightening). At early times during the 2015 May event, the 2000 km s^{-1} gas is hot and generates the 2000 km s^{-1} wide emission lines. Later on this relatively dense gas cools, and we detect a P-Cygni profile with two absorption features at 1000 and 2000 km s^{-1}. In this case, the 1000 km s^{-1} absorption is likely tracing material ejected during the 2013 event or earlier. If the star exploded as an SN in 2015 May (with velocities of about 10,000 km s^{-1}), the SN ejecta will reach the CSM shells after a few weeks.

Alternatively, it is possible that the 2015 May event released material at 2000 km s^{-1} that at early times is seen in emission and later in absorption. If this scenario is correct, we predict that X-ray and radio emission will not be detected, since the shock velocity is too low. The current X-ray nondetection, the reddening (cooling) of the spectra, and the lack of broad spectral features suggest that the star has not exploded yet.

The scenarios we discuss do not cover all possibilities. For example, breaking the spherical symmetry gives rise to a large number of scenarios. However, these are very hard to constrain given the limited information at hand. We stress that the observations are hardly conclusive, and it is still not clear what the nature of the 2015 May transient is. We note that future *HST* observations, taken after the transient light fades away, may check if the progenitor is still visible, and hence whether the 2015 May event marked the final explosion of the star.

3.3. The Radiative Efficiency of Precursors

Table 6 lists the measured properties of the precursor and the possible SN explosion. These properties were estimated based on the PTF light curve, the spectra, the *Swift*-UVOT data, and the *HST* observations (Elias-Rosa et al. 2015). Next, we use these properties to estimate the radiative efficiency of the precursor. The goal of this section is to roughly estimate the CSM mass ejected in the 2013 outburst, and to estimate the ratio between the radiated luminosity and kinetic energy of the precursor. This measurement has the potential to resolve the key question: what drives the CSM ejection? For example, a ratio much smaller than one favors models in which the radiation is generated by conversion of the kinetic energy of the ejected mass to radiation via interaction (forming collisonless shocks; e.g., Katz et al. 2011; Murase et al. 2011, 2014) with previously emitted material, over models in which a super-Eddington luminosity drives the ejection of the CSM.

Since the precursor has super-Eddington luminosity (for a $\lesssim$100 $M_{\odot}$ progenitor), it is likely that the outburst was associated with mass ejection. Here we attempt to estimate the physical parameters of the precursor (e.g., ejected mass) and to use it to estimate the ratio of the radiated energy of the precursor to its kinetic energy, which we call the precursor radiative efficiency:

$$\epsilon_R \equiv \frac{2\int L dt}{M_{\rm CSM} v_{\rm CSM}^2} \approx 3\times 10^{-3}\left(\frac{\langle L\rangle}{1.7\times 10^{40}\ {\rm erg\ s^{-1}}}\right)\left(\frac{\Delta t}{20\ {\rm day}}\right) \times \left(\frac{M_{\rm CSM}}{M_{\odot}}\right)^{-1}\left(\frac{v_{\rm CSM}}{1000\ {\rm km\ s^{-1}}}\right)^{-2}. \quad (2)$$

Here, L is the precursor luminosity as a function of time t, Δt is the precursor duration, $M_{\rm CSM}$ is the precursor ejecta mass, and $v_{\rm CSM}$ is the precursor ejecta velocity. The CSM mass can be expressed as

$$M_{\rm CSM} = \left(\frac{1}{\epsilon_R}\right)\left(\frac{2\langle L\rangle \Delta t}{v_{\rm CSM}^2}\right). \quad (3)$$

The radiative efficiency allows us to relate between the observed luminosity integrated over time, the CSM velocity, and mass. Furthermore, the exact value of the radiative efficiency likely depends on the CSM ejection mechanism, and therefore it may be useful for testing some theoretical ideas regarding the precursor physical mechanism (see Section 3.4).

However, our derivation is an order-of-magnitude estimate that relies on several assumptions, which are not necessarily correct. For example, we assume that the CSM has spherical symmetry and is not heavily clumped. Nevertheless, as far as we know, this is the only existing estimate for the radiative efficiency of a precursor.

The distance the precursor ejecta can travel during its 20 days ejection is

$$r_{\rm CSM} \approx v_{\rm CSM}\Delta t \approx 1.7\times 10^{14}\left(\frac{v_{\rm CSM}}{1000\ {\rm km\ s^{-1}}}\right)\left(\frac{\Delta t}{20\ {\rm days}}\right){\rm cm}, \quad (4)$$

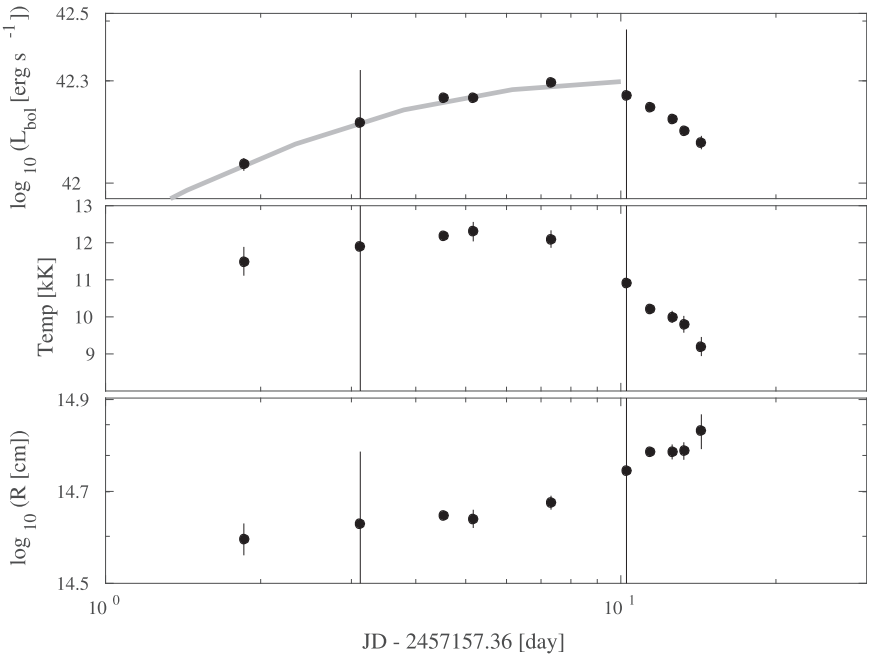

Figure 6. Fitted bolometric luminosity (upper panel), effective temperature (middle panel), and effective radius (lower panel) as a function of time since the fitted t_0. See the text for details. The gray line shows the best-fit exponential rise timescale.

Table 4
Swift-UVOT Bolometric Light Curve

JD − t_0	$L_{\rm bol}$	Temp.	Radius
(day)	($\times 10^{42}$ erg s^{-1})	(K)	($\times 10^{14}$ cm)
1.860	1.14 ± 0.05	11,500 ± 600	4.0 ± 0.5
3.126	1.50 ± 0.03	11,900 ± 300	4.3 ± 0.2
4.540	1.78 ± 0.02	12,200 ± 100	4.4 ± 0.1
5.176	1.79 ± 0.36	12,300 ± 600	4.4 ± 1.7
7.325	1.98 ± 0.04	12,100 ± 200	4.7 ± 0.2
10.260	1.81 ± 0.03	10,900 ± 200	5.5 ± 0.2
11.416	1.67 ± 0.04	10,200 ± 200	6.1 ± 0.3
12.582	1.54 ± 0.04	10,000 ± 300	6.1 ± 0.4
13.257	1.43 ± 0.04	9800 ± 200	6.1 ± 0.3
14.335	1.32 ± 0.05	9200 ± 300	6.8 ± 0.5

Note. Bolometric luminosity, effective temperature, and radius estimated from a blackbody fit to the *Swift*-UVOT observations (Table 3) corrected for Galactic extinction. Just as in Table 2, the temperature measurements should be regarded as lower limits on the effective temperature. Assuming the host extinction is twice as large as the Galactic extinction (i.e., as suggested by the Na I absorption doublet), the lower limit on the temperature will be higher by up to about 1000 K.

where Δt is the duration of the precursor ($\geqslant$20 days). An order-of-magnitude estimate of the mean density of the ejected CSM (during its ejection) is

$$n \approx \frac{M_{\rm CSM}}{\mu_{\rm p} m_{\rm p} 4/3 \pi r_{\rm CSM}^3} \approx 2.7 \times 10^{11} \left(\frac{1}{\epsilon_R}\right)\left(\frac{\langle L\rangle}{1.7\times 10^{40}\ {\rm erg\ s^{-1}}}\right)\left(\frac{\mu_{\rm p}}{0.6}\right)^{-1} \times \left(\frac{\Delta t}{20\ {\rm day}}\right)^{-2}\left(\frac{v_{\rm CSM}}{1000\ {\rm km\ s^{-1}}}\right)^{-5} {\rm cm^{-3}}. \quad (5)$$

Here, $\mu_{\rm p}$ is the mean molecular weight (assumed to be 0.6).

Another constraint comes from the fact that the precursor radiation disappeared on a timescale shorter than one week (Figure 2); thus, the cooling timescale is $\lesssim$1 week. The Bremsstrahlung cooling timescale, which gives an upper limit on the cooling timescale, is given by

$$t_{\rm cool} \lesssim 1.76 \times 10^{13} \left(\frac{T}{10^4\ {\rm K}}\right)^{1/2}\left(\frac{n}{1\ {\rm cm^{-3}}}\right)^{-1} \times \left(\frac{Z}{1}\right)^{-2} {\rm s}, \quad (6)$$

where T is the gas temperature and Z is the atomic number (number of protons), and thus can be translated to a lower limit on the density of the emitting region. If we require that $t_{\rm cool} < 7$ days, and assume $\langle Z\rangle \approx 1.7$ and $T \approx 10^4$ K, we find that $n \gtrsim 7 \times 10^7$ cm^{-3}. Combining this limit on n along with Equation (5) and the fact that $\Delta t \geqslant 20$ days, we get

$$\epsilon_R \lesssim 3.4 \times 10^3. \quad (7)$$

Next, an order-of-magnitude estimate for the photon diffusion timescale (e.g., Popov 1993; Padmanabhan 2001) is given by

$$t_{\rm diff} \approx \frac{9\kappa M_{\rm CSM}}{4\pi^3 c r_{\rm CSM}} \approx 0.32 \left(\frac{1}{\epsilon_R}\right)\left(\frac{\kappa}{0.34\ {\rm cm\ gr^{-1}}}\right)\left(\frac{\langle L\rangle}{1.7\times 10^{40}\ {\rm erg\ s^{-1}}}\right) \times \left(\frac{v_{\rm CSM}}{1000\ {\rm km\ s^{-1}}}\right)^{-3} {\rm day}. \quad (8)$$

Assuming that $t_{\rm diff} \lesssim 7$ days, we can set the following lower limit:

$$\epsilon_R \gtrsim 0.04. \quad (9)$$

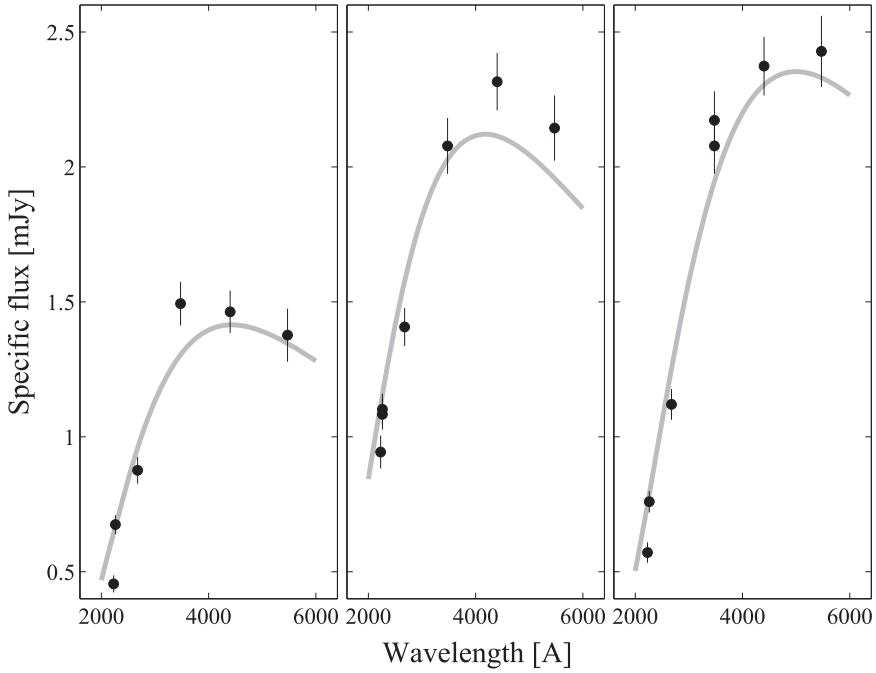

Figure 7. From left to right, we present the UVOT spectral energy distribution of SN Hunt 275, on three epochs: 1.8, 4.5, and 14.3 days after t_0, respectively. The gray lines represent the best-fit blackbody curve.

Table 5
Swift-XRT observations

JD − t_0 (day)	Exp. Time (s)	Source (counts)	Background (counts)
−2685.835	9595.4	2	38
−2682.295	4563.3	1	55
−2680.750	28649.6	3	124
−2679.740	11428.2	2	28
−2678.811	15785.9	0	65

Note. Source is the number of counts in a 9″-radius aperture of the source position and in the 0.2–10 keV band. Background is the number of counts, in the 0.2–10 keV band, in an annulus of inner (outer) radius of 50″ (100″) around the source. The ratio between the background annulus area and the aperture area is 92.59.

(This table is available in its entirety in machine-readable form.)

Table 6
PTF 13efv and SNHunt 275 Observed Properties

Property	Value
Progenitor luminosity (*HST* observations)	$(2-7)\times10^{39}$ erg s^{-1}
Precursor *R*-band peak luminosity	1.7×10^{40} erg s^{-1}
Precursor peak *R*-band absolute mag	−11.9 mag
Precursor total integrated radiated *R*-band	$>2.4\times10^{46}$ erg
Precursor duration	>20 days
Precursor decay timescale	< 7 days
Precursor time before the explosion	∼500 days
Precursor velocity from P-Cygni profile	∼1000 km s^{-1}
UM2 − R (AB) color index	>1.4 mag
2015 May event rise timescale	2.2 ± 1.6 days
2015 May event peak bolometric luminosity	$\sim2\times10^{42}$ erg s^{-1}
2015 May event integrated bolometric radiation	$\sim1.8\times10^{48}$ erg

Note. Properties of the progenitor (upper block), 2013 December precursor event (middle block), and 2015 May event (lower block). The blocks are separated by horizontal lines.

Until now, our constraints on the radiative efficiency are based on the properties of the precursor. Next, we will use the properties of the 2015 May event to derive additional constraints.

Assuming $v_{\rm CSM}\approx1000$ km s^{-1}, after 500 days (i.e., the time between the 2013 December precursor and the 2015 May event), the CSM traveled a distance of $r_{\rm CSM}\approx4\times10^{15}$ cm. Since the rise time of the 2015 May event is about 2 days (Table 6), we can use the diffusion timescale (Equation (8)) to set an order-of-magnitude upper limit on the mass of the CSM:

$$M_{\rm CSM}\lesssim0.4\left(\frac{t_{\rm diff}}{2\ {\rm day}}\right)\left(\frac{r_{\rm CSM}}{4\times10^{15}\ {\rm cm}}\right)\times\left(\frac{\kappa}{0.34\ {\rm cm\ g^{-1}}}\right)^{-1}M_{\odot}. \quad (10)$$

Inserting this limit on $M_{\rm CSM}$ into Equation (2) gives

$$\epsilon_R\gtrsim0.007\left(\frac{\Delta t}{20\ {\rm day}}\right)\left(\frac{v_{\rm CSM}}{1000\ {\rm km\ s^{-1}}}\right)^{-2}. \quad (11)$$

We note that currently we also have the following upper limit on the duration and luminosity of the precursor. Since we did not find a transient at the location of PTF 13efv in the Catalina Real Time Survey[15] (CRTS; Drake et al. 2009), and assuming CRTS can detect magnitude 19 transients, we can conclude that the luminosity of the precursor was not larger by more than a factor of about four than the observed luminosity of 1.7×10^{40} erg s^{-1} seen during 2013 December. Furthermore, the PTF *g*-band nondetection prior to the 2013 December event sets an upper limit of about 240 days on Δt. Since the precursor was not detected in the UV (Table 6), the bolometric correction is likely small.

[15] http://nunuku.caltech.edu/cgi-bin/getcssconedb_release_img.cgi

To conclude, combining all the constraints, we set the following limits on the radiative efficiency:

$$0.04 \lesssim \epsilon_R \lesssim 3400. \quad (12)$$

We stress that this is an order-of-magnitude estimate and it includes several assumptions that are not necessarily correct. Therefore, the results of this analysis should be viewed with caution. Since we cannot determine whether the efficiency is smaller or larger than unity, we cannot point definitively toward one of two types of scenarios: kinetic energy converted into radiation or radiation-driven mass-loss. However, with improved observational constraints this analysis can be used in the future to obtain better estimates of the radiative efficiency of precursors.

3.4. What Drives the Mass Loss and Radiation?

In the case that the 2013 event is caused by a super-Eddington continuum-driven wind, we expect that it will satisfy a mass-loss versus luminosity relation. In this case, Shaviv (2001) has shown that the total mass-loss is given by

$$M \approx \mathcal{W}\frac{L - L_{\rm Edd}}{c\ c_{\rm s}}\Delta t, \quad (13)$$

where $\mathcal{W}$ is a dimensionless constant that empirically was found to be of the order of a few, $c_{\rm s}$ is the speed of sound at the base of the wind (estimated to be $60\,{\rm km\,s^{-1}}$), and $L_{\rm Edd}$ is the Eddington luminosity. For $L \gg L_{\rm Edd}$ we can write

$$M \approx 4 \times 10^{-5}\left(\frac{\mathcal{W}}{5}\right) \times \left(\frac{L}{1.7 \times 10^{40}\ {\rm erg\ s^{-1}}}\right)\left(\frac{\Delta t}{20\ {\rm day}}\right) M_{\odot}. \quad (14)$$

This estimate is below the derived upper limits on the CSM mass, and hence we cannot rule out this model.

The second option that we would like to consider is that the radiation is generated from conversion of the kinetic energy of the ejected mass to radiation via interaction with previously emitted material (e.g., Smith et al. 2014). One possible problem with this scenario is that the interaction will produce mostly hard X-ray photons (e.g., Fransson 1982; Katz et al. 2011; Murase et al. 2011, 2014; Chevalier & Irwin 2012; Svirski et al. 2012). Presumably, it is possible to convert these X-ray photons to visible light by Comptonization or bound-free absorption (e.g., Chevalier & Irwin 2012; Svirski et al. 2012). Comptonization requires larger than unity Thompson optical depth, while the bound-free absorption will need neutral CSM mass with column densities above $\sim 10^{23}\ {\rm cm^{-2}}$. We note that in the current observations there is no evidence for a large Thompson optical depth, but we cannot rule out strong bound-free absorption. Moreover, this scenario may still work, if we introduce large departures from the spherical symmetry that we have assumed so far.

4. SUMMARY

We present observations of a precursor, peaking at an absolute magnitude of about -12, $\sim$500 days prior to the SNHunt 275 2015 May event. Also included are *Swift*-UVOT observations of the 2015 May event that peaked at an absolute magnitude of -17. We discuss the nature of the 2015 May event, and conclude that it is not yet clear whether this event signals the final explosion of the progenitor or is still another eruption. If the latter, then we may detect an SN taking place within months to a few years.

Finally, we use the observations to constrain the ratio of the radiated energy to the kinetic energy of the precursor (i.e., the radiative efficiency). Under some simplistic assumptions, our order-of-magnitude estimate suggests that the radiative efficiency of PTF 13efv is $\gtrsim$0.04. However, this still does not necessarily mean that all precursors have similar radiative efficiencies.

We thank M. Graham, P. Kelly, A. Bostroem, I. Shivvers, and W. Zheng for their help obtaining some of the optical spectra. We are also grateful to the staffs of the Palomar, Lick, and Keck Observatories for their excellent assistance. Research at Lick Observatory is partially supported by a generous gift from Google. Some of the data presented herein were obtained at the W.M. Keck Observatory, which is operated as a scientific partnership among the California Institute of Technology, the University of California, and NASA; the observatory was made possible by the generous financial support of the W.M. Keck Foundation. The authors wish to recognize and acknowledge the very significant cultural role and reverence that the summit of Mauna Kea has always had within the indigenous Hawaiian community. We are most fortunate to have the opportunity to conduct observations from this mountain. E.O.O. is the incumbent of the Arye Dissentshik career development chair and is grateful for support by grants from the Willner Family Leadership Institute Ilan Gluzman (Secaucus NJ), the Israel Science Foundation, Minerva, Weizmann-UK, and the I-Core program by the Israeli Committee for Planning and Budgeting and the Israel Science Foundation (ISF). N.J.S. is grateful for the IBM Einstein Fellowship. A.G.Y. is supported by the EU/FP7 via ERC grant No. 307260, the Quantum universe I-Core program by the Israeli Committee for Planning and Budgeting and the ISF; by Minerva and ISF grants; by the Weizmann-UK "making connections" program; and by Kimmel and ARCHES awards. M.S. acknowledges support from the Royal Society and EU/FP7-ERC grant No. 615929. A.V.F.'s research is supported by the Christopher R. Redlich Fund, the TABASGO Foundation, and NSF grant AST-1211916.

REFERENCES

Arnett, W. D., & Meakin, C. 2011, ApJ, 741, 33
Bilinski, C., Smith, N., Li, W., et al. 2015, MNRAS, 450, 246
Brown, P. J., Holland, S. T., Immler, S., et al. 2009, AJ, 137, 4517
Campana, S., Thoene, C. C., Leloudas, G., Aceituno, F., & Postigo, A. d. U. 2015, ATel, 7517, 1
Cardelli, J. A., Clayton, G. C., & Mathis, J. S. 1989, ApJ, 345, 245
Chevalier, R. A. 2012, ApJL, 752, L2
Chevalier, R. A., & Irwin, C. M. 2012, arXiv:1201.5581
Chugai, N. N., & Danziger, I. J. 1994, MNRAS, 268, 173
Corsi, A., Ofek, E. O., Gal-Yam, A., et al. 2014, ApJ, 782, 42
de Ugarte Postigo, A. d. U., Leloudas, G., & Thoene, C. C. 2015a, ATel, 7409, 1
de Ugarte Postigo, A. d. U., Thoene, C. C., Leloudas, G., & Aceituno, F. 2015b, ATel, 7514, 1
de Ugarte Postigo, A. d. U., Thoene, C. C., Leloudas, G., & Aceituno, F. 2015c, ATel, 7517, 1
Drake, A. J., Djorgovski, S. G., Mahabal, A., et al. 2009, ApJ, 696, 870
Duggan, G., Bellm, E., Leloudas, G., et al. 2015, ATel, 7515, 1
Efron, B. 1982, in CBMS-NSF Regional Conf. Ser. in Applied Mathematics (Philadelphia: Society for Industrial and Applied Mathematics (SIAM))
Elias-Rosa, N., Benetti, S., Tomasella, L., et al. 2015, ATel, 7042, 1

Faber, S. M., Phillips, A. C., Kibrick, R. I., et al. 2003, Proc. of SPIE, 4841, 1657
Fassia, A., Meikle, W. P. S., Chugai, N., et al. 2001, MNRAS, 325, 907
Filippenko, A. V. 1991, in European Southern Observatory Conf. and Workshop Proc. 37 (Garching: ESO), 343
Filippenko, A. V. 1997, ARA&A, 35, 309
Firth, R. E., Sullivan, M., Gal-Yam, A., et al. 2015, MNRAS, 446, 3895
Foley, R. J., Smith, N., Ganeshalingam, M., et al. 2007, ApJL, 657, L105
Fransson, C. 1982, A&A, 111, 140
Fraser, M., Kotak, R., Pastorello, A., et al. 2015, MNRAS, 453, 3886
Fraser, M., Magee, M., Kotak, R., et al. 2013, ApJL, 779, L8
Gal-Yam, A., Arcavi, I., Ofek, E. O., et al. 2014, Natur, 509, 471
Gehrels, N., Chincarini, G., Giommi, P., et al. 2004, ApJ, 611, 1005
Groh, J. H. 2014, A&A, 572, L11
Hook, I., Jorgensen, I., Allington-Smith, J. R., et al. 2004, PASP, 116, 425
Katz, B., Sapir, N., & Waxman, E. 2011, arXiv:1106.1898
Khazov, D., Yaron, O., Gal-Yam, A., et al. 2016, ApJ, 818, 3
Kiewe, M., Gal-Yam, A., Arcavi, I., et al. 2012, ApJ, 744, 10
Laher, R. R., Surace, J., Grillmair, C. J., et al. 2014, PASP, 126, 674
Law, N. M., Kulkarni, S. R., Dekany, R. G., et al. 2009, PASP, 121, 1395
Margutti, R., Milisavljevic, D., Soderberg, A. M., et al. 2014, ApJ, 780, 21
Matheson, T., Filippenko, A. V., Ho, L. C., Barth, A. J., & Leonard, D. C. 2000, AJ, 120, 1499
Mauerhan, J. C., Smith, N., Filippenko, A. V., et al. 2013, MNRAS, 430, 1801
Miller, J. S., & Stone, R. P. S. 1993, Lick Observatory Tech. Rep. 66, (Santa Cruz, CA: Lick Observatory)
Modjaz, M., Li, W., Butler, N., et al. 2009, ApJ, 702, 226
Moretti, A., Campana, S., Tagliaferri, G., et al. 2004, Proc. SPIE, 5165, 232
Moriya, T. J., & Langer, N. 2015, A&A, 573, A18
Murase, K., Thompson, T. A., Lacki, B. C., & Beacom, J. F. 2011, PhRvD, 84, 043003
Murase, K., Thompson, T. A., & Ofek, E. O. 2014, MNRAS, 440, 2528
Niemela, V. S., Ruiz, M. T., & Phillips, M. M. 1985, ApJ, 289, 52
Ofek, E. O. 2014, Astrophysics Source Code Library, ascl:1407.005
Ofek, E. O., Arcavi, I., Tal, D., et al. 2014c, ApJ, 788, 154
Ofek, E. O., Laher, R., Law, N., et al. 2012a, PASP, 124, 62
Ofek, E. O., Laher, R., Surace, J., et al. 2012b, PASP, 124, 854
Ofek, E. O., Lin, L., Kouveliotou, C., et al. 2013a, ApJ, 768, 47
Ofek, E. O., Sullivan, M., Cenko, S. B., et al. 2013b, Natur, 494, 65
Ofek, E. O., Sullivan, M., Shaviv, N. J., et al. 2014a, ApJ, 789, 104
Ofek, E. O., Zoglauer, A., Boggs, S. E., et al. 2014b, ApJ, 781, 42
Oke, J. ,B., Cohen, J. ,G., Carr, M., et al. 1995, PASP, 107, 375
Oke, J. B., & Gunn, J. E. 1983, ApJ, 266, 713
Padmanabhan, T. 2001, Stars and Stellar Systems Theoretical Astrophysics, Vol. 2 (Cambridge: Cambridge Univ. Press)
Pastorello, A., Cappellaro, E., Inserra, C., et al. 2013, ApJ, 767, 1
Pastorello, A., Della Valle, M., Smartt, S. J., et al. 2007, Natur, 449, 1
Pastorello, A., Mattila, S., Zampieri, L., et al. 2008, MNRAS, 389, 113
Poole, T. S., Breeveld, A. A., Page, M. J., et al. 2008, MNRAS, 383, 627
Popov, D. V. 1993, ApJ, 414, 712
Prieto, J. L., Brimacombe, J., Drake, A. J., & Howerton, S. 2013, ApJL, 763, L27
Quataert, E., & Shiode, J. 2012, MNRAS, 423, L92
Rakavy, G., Shaviv, G., & Zinamon, Z. 1967, ApJ, 150, 131
Rau, A., Kulkarni, S. R., Law, N. M., et al. 2009, PASP, 121, 1334
Roming, P. W. A., Kennedy, T. E., Mason, K. O., et al. 2005, SSRv, 120, 95
Schlegel, D. J., Finkbeiner, D. P., & Davis, M. 1998, ApJ, 500, 525
Schlegel, E. M. 1990, MNRAS, 244, 269
Shaviv, N. J. 2000, ApJL, 532, L137
Shaviv, N. J. 2001, MNRAS, 326, 126
Shiode, J. H., & Quataert, E. 2014, ApJ, 780, 96
Shivvers, I., Groh, J. H., Mauerhan, J. C., et al. 2015, ApJ, 806, 213
Silverman, J. M., Foley, R. J., Filippenko, A. V., et al. 2012, MNRAS, 425, 1789
Smith, N. 2013, MNRAS, 429, 2366
Smith, N., Mauerhan, J. C., Cenko, S. B., et al. 2015, MNRAS, 449, 1876
Smith, N., Mauerhan, J. C., & Prieto, J. L. 2014, MNRAS, 438, 1191
Smith, N., Miller, A., Li, W., et al. 2010, AJ, 139, 1451
Soderberg, A. M., Berger, E., Page, K. L., et al. 2008, Natur, 453, 469
Soker, N., & Kashi, A. 2013, ApJL, 764, L6
Strotjohann, N. L., Ofek, E. O., Gal-Yam, A., et al. 2015, ApJ, 811, 117
Svirski, G., Nakar, E., & Sari, R. 2012, arXiv:1202.3437
Thöne, C. C., Michałowski, M. J., Leloudas, G., et al. 2009, ApJ, 698, 1307
Van Dyk, S. D., & Matheson, T. 2012, Astrophysics and Space Science Library, 384, 249
Vinko, J., Sarneczky, K., & Vida, K. 2015, ATel, 7541, 1
Waldman, R. 2008, ApJ, 685, 1103
Woosley, S. E., Blinnikov, S., & Heger, A. 2007, Natur, 450, 390
Yaron, O., & Gal-Yam, A. 2012, PASP, 124, 668
Yaron, O., Perley, D., & Gal-Yam, A. 2016, submitted
Zackay, B., & Ofek, E. O. 2015a, arXiv:1512.06872
Zackay, B., & Ofek, E. O. 2015b, arXiv:1512.06879
Zackay, B., Ofek, E. O., & Gal-Yam, A. 2016, arXiv:1601.02655